

# Near-Infrared and Short-Wavelength Infrared Photodiodes Based on Dye–Perovskite Composites

Qianqian Lin, Zhiping Wang, Margaret Young, Jay B. Patel, Rebecca L. Milot, Laura Martinez Maestro, Richard R. Lunt, Henry J. Snaith, Michael B. Johnston, and Laura M. Herz\*

Organohalide perovskites have emerged as promising light-sensing materials because of their superior optoelectronic properties and low-cost processing methods. Recently, perovskite-based photodetectors have successfully been demonstrated as both broadband and narrowband varieties. However, the photodetection bandwidth in perovskite-based photodetectors has so far been limited to the near-infrared regime owing to the relatively wide band gap of hybrid organohalide perovskites. In particular, short-wavelength infrared photodiodes operating beyond 1  $\mu\text{m}$  have not yet been realized with organohalide perovskites. In this study, narrow band gap organic dyes are combined with hybrid perovskites to form composite films as active photoresponsive layers. Tuning the dye loading allows for optimization of the spectral response characteristics and excellent charge-carrier mobilities near  $11 \text{ cm}^2 \text{ V}^{-1} \text{ s}^{-1}$ , suggesting that these composites combine the light-absorbing properties or IR dyes with the outstanding charge-extraction characteristics of the perovskite. This study demonstrates the first perovskite photodiodes with deep near-infrared and short-wavelength infrared response that extends as far as 1.6  $\mu\text{m}$ . All devices are solution-processed and exhibit relatively high responsivity, low dark current, and fast response at room temperature, making this approach highly attractive for next-generation light-detection techniques.

## 1. Introduction

The detection of light underpins modern science and technology, including imaging, surveillance, communication, biological sensing, and machine vision.<sup>[1–3]</sup> Most commercial


photodetectors are based on crystalline inorganic semiconductors, such as Si, GaAs, GaP, Ge, PbS, and InGaAs.<sup>[2,4]</sup> In particular, silicon is used for charge-coupled devices and sensors based on complementary metal–oxide–semiconductor technology, which dominate the current image-sensor market.<sup>[5]</sup> Silicon-based detectors are also extensively used in spectroscopy and advanced light detection systems. However, the photoresponse of such detectors is normally limited by the band gap of the active material, which leads to a long-wavelength cut-off around 1.1  $\mu\text{m}$ <sup>[6]</sup> for silicon-based devices. As an alternative, Ge, PbS, and InGaAs photodetectors have been introduced to allow detection of infrared light, albeit at substantially higher cost and cooling requirements to ensure high efficiency of photodetection. Hence, low-noise, efficient photodetectors with broad photoresponse covering the whole range of ultraviolet, visible, near-infrared (NIR,  $\approx 0.75\text{--}1 \mu\text{m}$ ), and short-wavelength infrared (SWIR,  $\approx 1\text{--}3 \mu\text{m}$ ) could play an

important role in advancing light sensing.<sup>[7–9]</sup>

Recently, solution-processed organic semiconductors,<sup>[10–12]</sup> quantum dots,<sup>[9,13,14]</sup> and organohalide perovskites (OHPs)<sup>[15–18]</sup> have emerged as promising candidates for next generation photodetection, combining the merits of low fabrication costs, tailorable optoelectronic properties, and excellent performance.<sup>[3]</sup> Photodetectors based on organohalide perovskites, in particular, have emerged over the last three years as a novel and highly promising technology, benefiting from the rapid progress in understanding of perovskite optoelectronics associated with their use in photovoltaic cells.<sup>[19,20]</sup> Many new OHPs combine the beneficial chemical properties of hybrid materials with extraordinary optoelectronic performance. Organic–inorganic lead halide perovskites can be easily solution-processed or thermally evaporated,<sup>[20,21]</sup> possess high electron and hole mobilities<sup>[22]</sup> and long charge-carrier diffusion lengths and lifetimes compared with other solution-processable semiconductors, allow for band-gap tuning through simple chemical substitutions, and are compatible with flexible platforms.<sup>[23,24]</sup> This collection of properties offers substantial benefits to the device performance of an OHP-based photodetector. For instance, high charge-carrier mobilities will result in a fast photoresponse; the tunable band gap allows control over

Dr. Q. Lin, Dr. Z. Wang, J. B. Patel, Dr. R. L. Milot,  
Dr. L. Martinez Maestro, Prof. H. J. Snaith,  
Prof. M. B. Johnston, Prof. L. M. Herz  
Clarendon Laboratory  
University of Oxford  
Parks Rd, Oxford OX1 3PU, UK  
E-mail: laura.herz@physics.ox.ac.uk

M. Young, Prof. R. R. Lunt  
Department of Chemical Engineering and Materials Science  
Michigan State University  
East Lansing, MI 48824, USA

 The ORCID identification number(s) for the author(s) of this article can be found under <https://doi.org/10.1002/adfm.201702485>.

© 2017 The Authors. Published by WILEY-VCH Verlag GmbH & Co. KGaA, Weinheim. This is an open access article under the terms of the Creative Commons Attribution License, which permits use, distribution and reproduction in any medium, provided the original work is properly cited.

DOI: 10.1002/adfm.201702485

the bandwidth of the photodetection; and low charge-carrier recombination rates and long diffusion lengths can offer large dynamic range and photoresponsivity.<sup>[25,26]</sup> High-performance perovskite photodetectors, including both broadband and narrowband versions, have been fabricated and shown to exhibit desirable performance.<sup>[27–30]</sup> More recently, efficient X-ray detectors,<sup>[31]</sup> photodetector arrays,<sup>[32]</sup> novel single-crystal<sup>[33]</sup> and nanowire<sup>[34]</sup>-based OHP photodetectors have also been realized.

Despite such rapid initial progress, the long-wavelength cut-off of the photoresponse bandwidth is still limited to date by the band gap of the OHPs. For hybrid organohalide perovskites, the longest wavelength currently reached is around 1000 nm, in a Sn–Pb binary-metal perovskite with a relatively small band gap of 1.28 eV.<sup>[35]</sup> More recently, Zhang et al. reported perovskite-erbium silicate nanosheet hybrid photodetectors based on a phototransistor architecture, achieving SWIR photoresponse with an on-set shifted out to 1.54  $\mu\text{m}$ .<sup>[36]</sup> However, phototransistors and photoresistors are normally limited by their relatively slow response time, while photodiodes are generally more favorable for high-speed applications. Furthermore, Lin et al.<sup>[26]</sup> and Teng et al.<sup>[37]</sup> recently reported large band-gap organic dyes with ionic nature, e.g., Rhodamine B that showed excellent mixing compatibility with hybrid perovskites and modified the absorption spectra of the perovskite active layer. Hence, we propose that exploiting this approach for dyes absorbing at long wavelengths beyond the perovskite band edge could offer an exciting new pathway to the realization of ultra-broadband photodiodes.

Motivated by these factors, we fabricate devices incorporating a set of ionic dyes with narrow band gaps embedded in the perovskite sensing layer to extend the light absorption deep

into the NIR and SWIR regimes. Owing to the excellent optoelectronic properties, the perovskite host is expected to facilitate charge transport to the electrodes. Spectroscopic investigations indeed reveal excellent optoelectronic properties of these dye–perovskite composites, such as high charge-carrier mobilities and nanosecond lifetimes suitable for efficient charge-carrier extraction. We further demonstrate the operation of dye–perovskite composite photodiodes with good responsivity, dark current, and noise characteristics that cover both the visible and infrared spectral range up to 1.6  $\mu\text{m}$ .

## 2. Results and Discussion

### 2.1. Dye-Perovskite Composite Films

Prior to the fabrication of photodetectors, the structural and optoelectronic properties of dye–perovskite thin-film composites are investigated. In this work, a mixed-cation lead mixed-halide perovskite,  $\text{FA}_{0.83}\text{Cs}_{0.17}\text{Pb}(\text{I}_{0.9}\text{Br}_{0.1})_3$ , is chosen as an active sensing layer because of its enhanced stability and superior optoelectronic properties.<sup>[38,39]</sup> Figure 1a schematically depicts the perovskite structure of  $\text{FA}_{0.83}\text{Cs}_{0.17}\text{Pb}(\text{I}_{0.9}\text{Br}_{0.1})_3$ . In this stoichiometry, the use of the FA-Cs cation mixture leads to an effective ionic radius that fits well within the Goldschmidt tolerance range, stabilizing the structure against deterioration into non-perovskite phases that are not photoactive.<sup>[40,41]</sup> The band gap of this perovskite is predominantly influenced by the lead halide octahedral cages, and therefore by the ratio between iodide and bromide content.<sup>[42]</sup> Here, we fix the I:Br ratio at 9:1 to achieve a smaller band gap (1.55 eV), i.e., a somewhat larger photo-detection bandwidth than for the corresponding pristine iodide

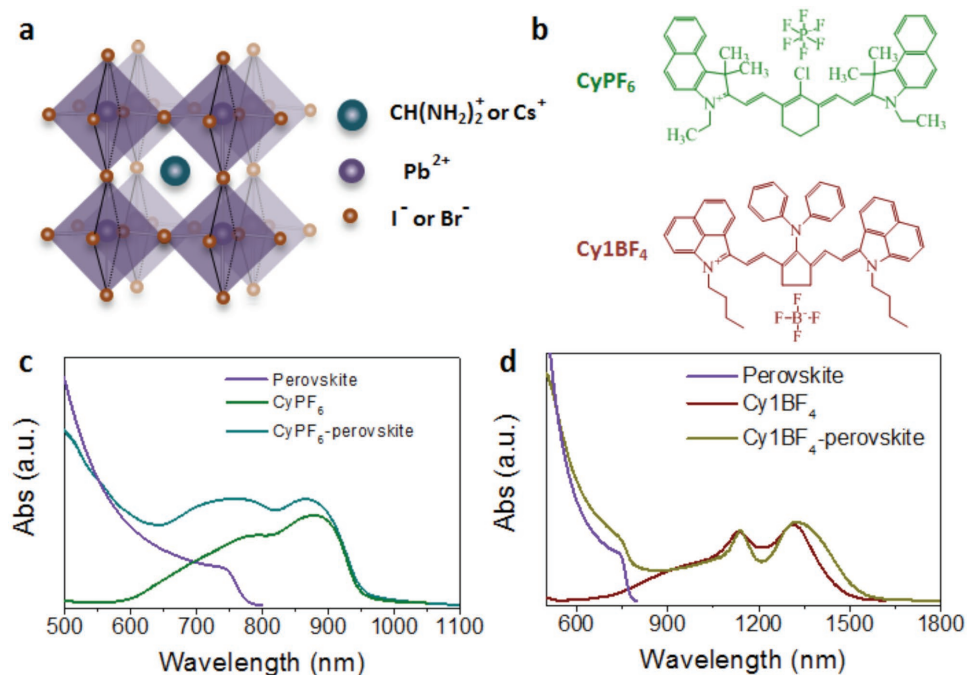


**Figure 1.** a) Schematic structure of  $\text{FA}_{0.83}\text{Cs}_{0.17}\text{Pb}(\text{I}_{0.9}\text{Br}_{0.1})_3$  perovskite, b) chemical structure of dyes  $\text{CyPF}_6$  and  $\text{Cy1BF}_4$ , c) thin-film absorption spectra of  $\text{CyPF}_6$  and  $\text{CyPF}_6$ -perovskite composite (2:1), and d) absorption spectra of  $\text{Cy1BF}_4$  and  $\text{Cy1BF}_4$ -perovskite composite (2:1).

perovskite. Figure 1b displays the chemical structures of the dyes mixed with the perovskite active layer as complementary photoabsorbers, which are 2-[2-[2-chloro-3-[2-(1,3-dihydro-3,3-dimethyl-1-ethyl-2H-benz[e]indol-2-ylidene) ethylidene]-1-cylohexen-1-yl]-ethenyl]-3,3-dimethyl-1-ethyl-1H-benz[e]indolium hexafluoro-phosphate (CyPF<sub>6</sub>) and 1-Butyl-2-(2-[3-[2-(1-butyl-1H-benzo[cd]indol-2-ylidene)-ethylidene]-2-diphenylamino-cyclopent-1-enyl]-vinyl)-benzo[cd] indolium tetrafluoroborate (Cy1BF<sub>4</sub>). Importantly, both dyes are ionic and hydrophilic, and exhibit good compatibility with OHPs during thin film formation, with no observable aggregation or serious surface roughening of the thin film discernible by eye. Figure 1c,d shows the absorption spectra of dyes CyPF<sub>6</sub> and Cy1BF<sub>4</sub> along with those for the FA<sub>0.83</sub>Cs<sub>0.17</sub>Pb(I<sub>0.9</sub>Br<sub>0.1</sub>)<sub>3</sub> perovskite and the corresponding composite materials. Based on the rationale outlined above, the incorporated dyes are expected to harvest photons in the NIR and SWIR regimes. As expected, the absorption spectra of the composite thin films are a combination of the absorption features from the perovskite and the dyes, as shown in Figure 1c,d, and hence display significant absorption in the NIR and SWIR regimes. Furthermore, by controlling the blend ratio of the dye and perovskite, it is evidently possible to tailor the absorption spectra and consequently the photoresponse spectra.

## 2.2. Tuning Optoelectronic Properties through Dye Loading

To verify the tunability of the absorption spectra, we used CyPF<sub>6</sub>-perovskite composite films prepared with various blend ratios (volume to volume)—the corresponding absorbance

spectra were normalized to the film thickness and are shown in **Figure 2a**. As expected, the absorption in the NIR regime improves with increasing dye content, and the perovskite absorption attenuates commensurately. At blend ratios of 1:1 and 2:1, desirable absorption spectra with fairly even spectral response are achieved, which cover a broad range from 450 up to 1000 nm. The composite films with higher dye content (3:1 and 4:1 ratio) display only weak, broadened features in the region of the perovskite absorption (500–750 nm) implying that an excess of dye may inhibit perovskite crystallization. To identify the impact of dye loading on crystallinity, X-ray diffraction patterns of these films were recorded as shown in **Figure 2b**. Compared with the pristine perovskite film, the 1:1 composite film maintains the perovskite diffraction features around 14°, 20°, 24°, and 28°. However, the peaks exhibit lower intensity and broadened width compared to the pristine perovskite, indicating reduced crystallinity or crystallite size. This result is consistent with the broadening of the perovskite absorption features (**Figure 2a**) and is further confirmed by scanning electron microscope images that reveal a reduction in grain size upon dye loading (**Figure S1**, Supporting Information). The 3:1 composite films, on the other hand, exhibit typical “yellow phase” nonperovskite diffraction peaks at ≈12°,<sup>[43]</sup> suggesting that at high concentrations of the dye the formation of the perovskite structure is inhibited, which may deteriorate the charge transport property of the sensing layer (vide infra).

To further assess the photophysical properties of the composite films, photoluminescence (PL) spectra were taken for the dye CyPF<sub>6</sub>, the FA<sub>0.83</sub>Cs<sub>0.17</sub>Pb(I<sub>0.9</sub>Br<sub>0.1</sub>)<sub>3</sub> perovskite, and the CyPF<sub>6</sub>-perovskite (1:1) composite film as shown in **Figure 2c**. The pristine perovskite film shows a strong peak centered at

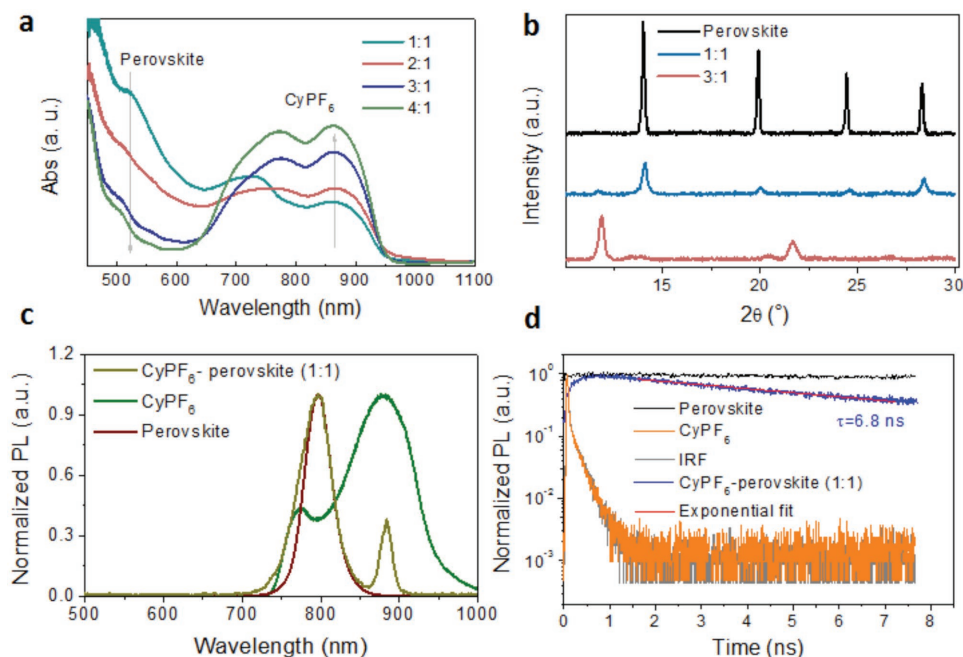


**Figure 2.** a) Thin-film absorption spectra of CyPF<sub>6</sub>-perovskite composites with various blend ratios, b) X-ray diffraction spectra of CyPF<sub>6</sub>-perovskite composites with various blend ratios, c) photoluminescence (PL) spectra of CyPF<sub>6</sub>, perovskite, and CyPF<sub>6</sub>-perovskite composite (1:1), and d) PL decay transients for CyPF<sub>6</sub>, perovskite, and CyPF<sub>6</sub>-perovskite composite. The films were excited at a wavelength of 400 nm; the PL was detected at a wavelength of 780 nm for the perovskite control and CyPF<sub>6</sub>-perovskite samples, and 900 nm for the CyPF<sub>6</sub> sample, respectively.

790 nm, which can be attributed to PL from the band edge. By comparison, the PL of CyPF<sub>6</sub> is not as intense, showing broad emission from 750 to 1000 nm. The PL spectrum of composite CyPF<sub>6</sub>-perovskite films comprises two distinct peaks: a CyPF<sub>6</sub> feature peak at 880 nm and a stronger perovskite feature located at the same wavelength as for the pristine perovskite films but having a larger full width at half maximum, most likely as a result of enhanced disorder. The composite films also exhibit more than two orders of magnitude lower PL intensity compared to the pristine perovskite film (Figure S2, Supporting Information), suggesting efficient PL quenching in the presence of CyPF<sub>6</sub> molecules. This behavior can be understood considering the energy levels of the dyes. Both CyPF<sub>6</sub> and Cy1BF<sub>4</sub> have relatively low highest occupied molecular orbital levels of -4.8 and -4.3 eV, respectively,<sup>[7,44]</sup> which enable efficient hole transfer from the perovskite to the dye (Figure S3, Supporting Information). Similarly, the positioning of the corresponding lowest unoccupied molecular orbital levels of the dyes will help electron extraction from the dyes to the perovskite. Such spatial segregation of electrons and holes in the different phases of the composite should therefore inhibit electron-hole recombination.

To probe the charge-carrier dynamics in these films, time-resolved PL transients were recorded using the time-correlated single photon counting (TCSPC) technique, as shown in Figure 2d and Figure S4 (Supporting Information). At the excitation fluence used, these dynamics are governed by monomolecular charge-carrier recombination with impurities that act as charge traps.<sup>[23]</sup> The pristine perovskite film shows a relatively long lifetime of ≈600 ns with a correspondingly small monomolecular rate constant  $k_1$  of  $1.7 \times 10^6 \text{ s}^{-1}$  (Figure S4, Supporting Information). These values are consistent with high-quality perovskite exhibiting a relatively low defect density.<sup>[41]</sup> The PL lifetime for CyPF<sub>6</sub> is found to be shorter than the resolution of the TCSPC system (≈200 ps) with the PL decay overlapping with the instrument response function. Importantly, for the CyPF<sub>6</sub>-perovskite composite films PL lifetimes of ≈7 ns ( $k_1 = 1.4 \times 10^8$ ) are found, which is much shorter than for the pristine perovskite film but substantially longer than for the dyes.

Optical-pump THz-probe photoconductivity spectroscopy (OPTP) was used to further probe the charge-carrier dynamics and charge transport properties of the CyPF<sub>6</sub>-perovskite composites (see the Supporting Information for details about OPTP data collection and analysis). Photoconductivity transients (Figure S5, Supporting Information) display significantly faster apparent higher-order recombination dynamics for the CyPF<sub>6</sub>-perovskite (1:1) composite than for the pristine perovskite. Fits to these data reveal effective bimolecular recombination rate constants that are higher by over an order of magnitude for the composite. These trends are again reflective of the smaller crystal grain sizes in the composite, as similar effects have been observed when moving from thin perovskite films to composites infused into mesoporous oxides, for which smaller perovskite grains form.<sup>[23,24]</sup> However, excellent charge-carrier mobility values are maintained provided the dye loading is not excessive. For the CyPF<sub>6</sub>-perovskite (1:1) composite we find a respectable electron-hole sum mobility of  $11 \text{ cm}^2 \text{ V}^{-1} \text{ s}^{-1}$ , only somewhat lower than that of the pristine perovskite control

( $20 \text{ cm}^2 \text{ V}^{-1} \text{ s}^{-1}$ ). For the CyPF<sub>6</sub>-perovskite (2:1) composite; however, the THz mobility drops to  $2 \text{ cm}^2 \text{ V}^{-1} \text{ s}^{-1}$ , suggesting that the dye loading is beginning to deteriorate charge percolation pathways. These charge-carrier mobility values are significantly above what would be expected for organic dye solids alone. Hence, we conclude that the incorporation of dyes into a hybrid perovskite matrix extends light absorption well into the SWIR region, while the perovskite host provides long charge-carrier lifetimes and high charge-carrier mobilities that result in improved charge transport and charge extraction, as shown below.

### 2.3. NIR and SWIR Photodiodes

Photodetector devices were fabricated using the dye-perovskite composites as photoactive layers. All photodiode devices were prepared with a planar architecture comprising a photoactive dye-perovskite layer sandwiched between a metal cathode and an indium tin oxide (ITO) transparent anode. Charge transport layers, i.e., [6,6]-Phenyl C<sub>61</sub> butyric acid methyl ester (PC<sub>61</sub>BM) and poly(3,4-ethylenedioxythiophene):polystyrene sulfonate (PEDOT:PSS), were also introduced to enhance the charge-carrier collection and suppress the dark current. The full device layer structure is ITO/PEDOT:PSS/dye-perovskite/PC<sub>61</sub>BM/Ag. By simply replacing the dye-perovskite active layer with pristine dye layers, control devices were fabricated for comparison.

It is well known that organic semiconductors have relatively low charge-carrier lifetimes, mobilities, and exciton diffusion lengths, which can limit organic semiconductor performance in homojunction devices when the film is “electrically” thick, i.e., the film is much thicker than the charge-carrier diffusion length.<sup>[26]</sup> However, “thick junctions” are preferable for manufacturing and device fabrication, which can reduce the probability of pin-holes, reduce the dark current and enhance the repeatability.<sup>[45]</sup> Not surprisingly, while a CyPF<sub>6</sub> control device with an active layer thickness of 80 nm can generate some photocurrent in the NIR regime, the responsivity values are extremely low (Figure 3c). Here, the low exciton diffusion length of typically ≈3 nm for an organic semiconductor clearly limits the usable range of neat layer thicknesses to ≈10 nm.<sup>[44]</sup> By contrast, Figure 3c also presents substantial enhancements by typically over an order of magnitude in responsivity when CyPF<sub>6</sub> is added into to the perovskite, even though a thicker active layer of ≈200 nm is now employed. Typically, the responsivity of the photodiodes increased from 0.8 to 24 mA W<sup>-1</sup> at 850 nm when the perovskite was added. This concept also shows that from the perspective of perovskite-only detectors, the response is now clearly extended to wavelengths where the perovskite by itself would not induce a photoresponse.<sup>[25]</sup>

To establish whether this concept could further be implemented for the SWIR spectral region beyond 1 μm, we fabricated photodiodes based on Cy1BF<sub>4</sub>-perovskite composites. As shown in Figure 3d, this low band gap dye contributes a substantial photoresponse from 800 to 1600 nm that again exceeds the responsivity of the Cy1BF<sub>4</sub> control device by an order of magnitude. The proof-of-concept for a solution-processable photodetector operating at room temperature up to 1600 nm is

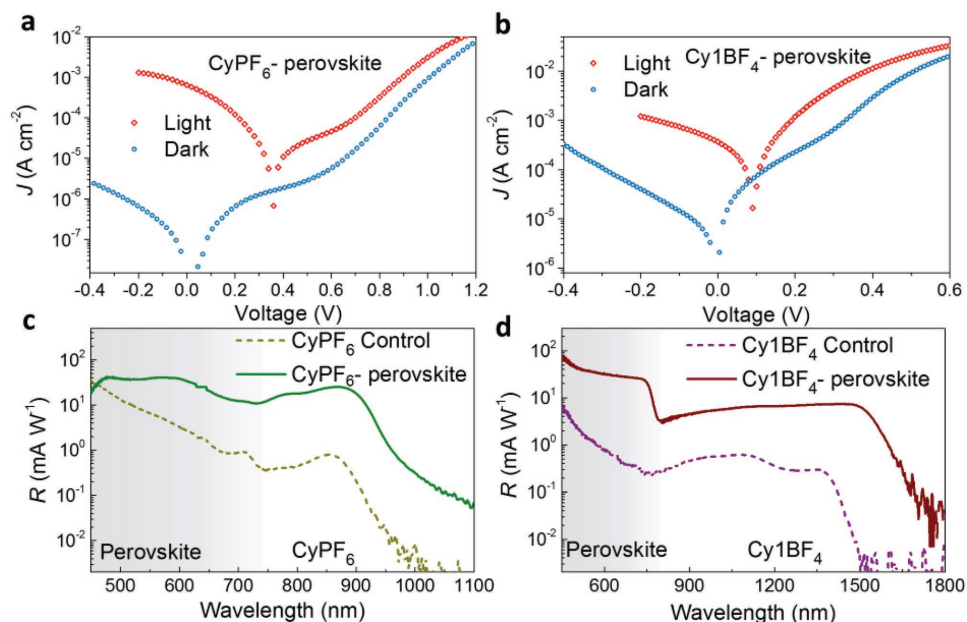


**Figure 3.** Comparison of device performance. a) Light and dark current density–voltage ( $J$ – $V$ ) curves of photodiodes based on  $\text{CyPF}_6$  and  $\text{CyPF}_6$ –perovskite composite (2:1), and b) light and dark current  $J$ – $V$  curves of photodiodes based on  $\text{Cy1BF}_4$  and  $\text{Cy1BF}_4$ –perovskite composite (2:1). c) Responsivity of photodiodes based on dye  $\text{CyPF}_6$  and  $\text{CyPF}_6$ –perovskite composite (2:1)—curves for other blend ratios are shown in Figure S4 of the Supporting Information, and d) responsivity of photodiodes based on dye  $\text{Cy1BF}_4$  and  $\text{Cy1BF}_4$ –perovskite composite (2:1).

particularly exciting as it allows for photon detection at typical fiber-optic communication wavelengths.

Overall, the extension of the photoresponse bandwidth to the NIR and SWIR regions of the spectrum validates our proposal of perovskite-dye composite photodiodes. Here, both components combine their advantageous properties, with the dye helping to absorb and utilize the NIR and SWIR photons, and the perovskite acting as an excellent host for efficient charge transport. In addition, this broadband perovskite photodetector concept with enhanced NIR and SWIR responsivities allows for further modulation of the responsivity spectra through changes in the dye-perovskite blend ratio, as shown in Figure S6a (Supporting Information). Interestingly, we also find that the responsivity can be enhanced slightly by application of a reverse bias of 0.5 V (Figure S6b, Supporting Information), perhaps through aiding exciton dissociation in the dye.

Finally, we examine the dark current as a critical component for photodetection, which is defined as the current flowing within the device in the absence of illumination. Figure 3a,b presents typical light and dark current–voltage ( $J$ – $V$ ) curves of the photodiodes based on  $\text{CyPF}_6$ –perovskite and  $\text{Cy1BF}_4$ –perovskite composite films, respectively. Normally, dark current and noise current sharply increase with decreasing band gap of the active material at any given temperature.<sup>[8]</sup> Compared with pristine perovskite photodiodes,<sup>[8]</sup> the  $\text{CyPF}_6$ –perovskite photodiodes still retain a relatively low room-temperature dark current of the order of  $0.01 \mu\text{A cm}^{-2}$  without bias, considering the low dye band gap of 1.25 eV. The SWIR photodiodes based on  $\text{Cy1BF}_4$ –perovskite exhibit much higher dark current of around  $2 \mu\text{A cm}^{-2}$  at zero bias which increases dramatically with increasing bias voltage, possibly due to the small band gap of  $\text{Cy1BF}_4$  of only 0.82 eV. The measured noise density

spectra (Figure S7, Supporting Information) of these two types of photodiodes show a trend similar to the dark current. The  $\text{Cy1BF}_4$ –perovskite based photodiode exhibits a higher noise density than that based on  $\text{CyPF}_6$ –perovskite, especially at  $-0.5$  V bias voltage (Figure S7, Supporting Information). From such accurate measurements of the responsivity and noise current, the noise equivalent power (NEP) and specific detectivity ( $D^*$ ) can be calculated.<sup>[25]</sup> The  $\text{CyPF}_6$ –perovskite based photodiodes achieved an NEP of  $\approx 1.5 \text{ nW Hz}^{1/2}$  and  $D^*$  of  $2 \times 10^8$  Jones at 900 nm without bias, and the  $\text{Cy1BF}_4$ –perovskite based devices demonstrate a slightly higher NEP of  $\approx 17 \text{ nW Hz}^{1/2}$  and lower  $D^*$  of  $2 \times 10^7$  Jones at 1500 nm (Figure S8, Supporting Information).

Another key performance metric is the frequency response, i.e., how fast the detector can respond to the input light signal, which sets the upper limit to the speed of image or data acquisition. As shown in Figure 4a, the typical  $-3$  dB point frequency ( $f_{-3 \text{ dB}}$ ) roll-off for  $\text{CyPF}_6$ –perovskite based photodiodes is around 65 kHz, while the  $\text{Cy1BF}_4$ –perovskite devices respond slightly faster, with  $f_{-3 \text{ dB}}$  of 85 kHz. Typical temporal response times of the  $\text{CyPF}_6$ –perovskite photodiodes are shown in Figure 4b, with a rise and fall time of 65 and 74  $\mu\text{s}$ , respectively, in good agreement with the measured frequency response. We note that these devices have relatively large ( $\approx 0.1 \text{ cm}^2$ ) and thin ( $\approx 150 \text{ nm}$ ) active layers, which results in considerable capacitance because of the high values of the dielectric function for hybrid metal halide perovskites.<sup>[25]</sup> It has been reported that the response time of perovskite photodiodes is mainly determined by the resistance–capacitance constants.<sup>[25]</sup> With reduced device area, faster photoresponses have been achieved by Shen et al.<sup>[16,46]</sup> However, the use of too small a device area may introduce substantial errors in the determination of the real active

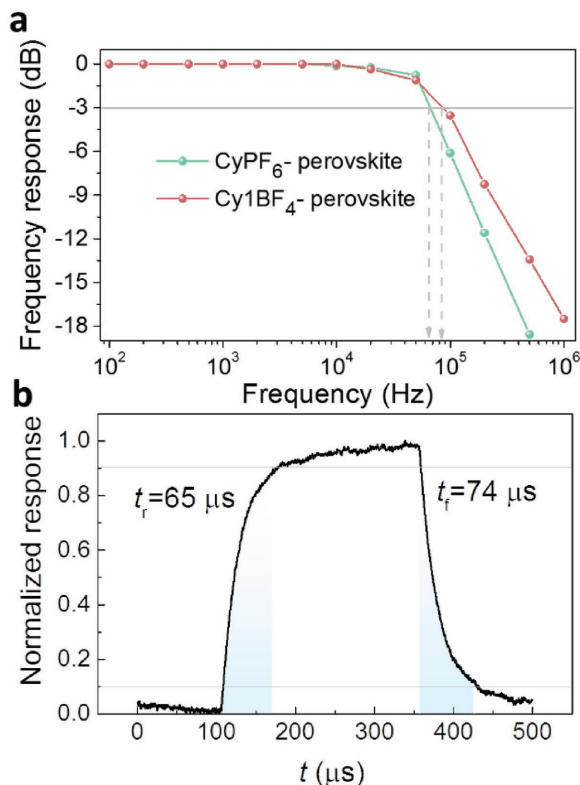


**Figure 4.** a) Typical frequency response of the NIR and SWIR photodiodes based on CyPF<sub>6</sub>-perovskite (2:1) and Cy1BF<sub>4</sub>-perovskite (2:1), respectively, and b) typical rise time and fall time of the NIR CyPF<sub>6</sub>-perovskite (2:1) photodiodes.

area, which will in turn affect the accuracy with which other device parameters can be calculated. To avoid such errors, we therefore decided to investigate devices with an active area of  $\approx 0.1 \text{ cm}^2$ . **Figure 5** further demonstrates the typical transient photoresponse of the Cy1BF<sub>4</sub>-perovskite photodiodes measured at wavelengths above and below the perovskite band gap. We highlight that a fast and highly repeatable response is obtained at SWIR wavelengths, and in particular well into the fiber-optic communications range. Figure S9 of the Supporting Information presents similar temporal response curves for the CyPF<sub>6</sub>-perovskite photodiodes in the NIR regime. Hence, this concept clearly allows for detection of photons below the band gap of hybrid metal halide perovskites, with low noise characteristics and fast response times.

### 3. Conclusion

In summary, we have demonstrated a novel method to extend the photoresponse bandwidth of perovskite photodetectors by blending dyes with suitable energetics into hybrid perovskites to create a composite active layer. Ionic, hydrophilic dyes compatible with perovskite solvents were found to allow for smooth film formation from a mixed precursor solution. Such mixed dye-perovskite composites combined the best of both ingredients, with the small band gap of the dyes enabling collection of NIR and SWIR photons and the perovskite crystals enhancing

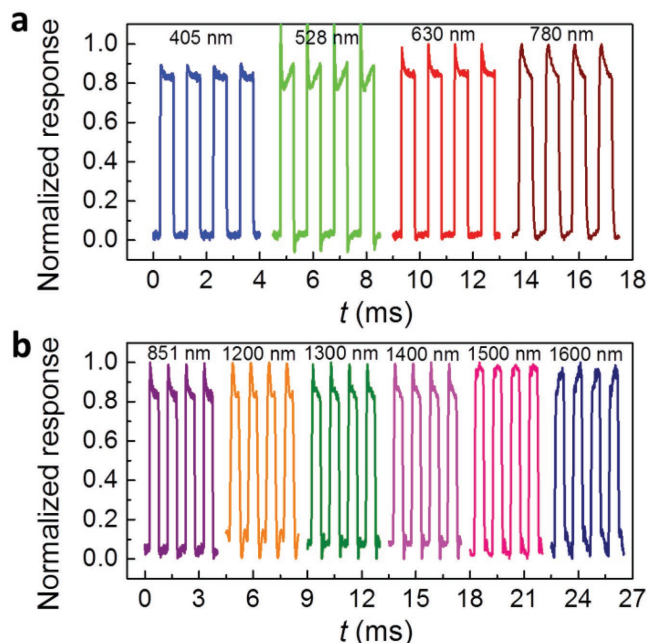


**Figure 5.** Temporal responses of the SWIR photodiode based on Cy1BF<sub>4</sub>-perovskite (2:1) to square-wave modulated light sources a) above and b) below the band gap of FA<sub>0.83</sub>CS<sub>0.17</sub>Pb(I<sub>0.9</sub>Br<sub>0.1</sub>)<sub>3</sub> perovskite. Corresponding curves for NIR CyPF<sub>6</sub>-perovskite (2:1) photodiodes are shown in the Supporting Information.

the charge transport in the active sensing layer. We further demonstrated that the optoelectronic properties of the composite films can be modulated with ease by control of the blend ratio. As a proof of concept, we fabricated prototype photodiodes based on the perovskite composite films which exhibit a broad-band photoresponse covering the majority of the visible, NIR and SWIR spectral ranges. These photodiodes display respectable responsivities in the range of 10–20 mA W<sup>-1</sup> across the NIR and SWIR regimes, with a response time of around 70  $\mu\text{s}$ , and good dark current and noise characteristics. We conclude that dye-perovskite composite photodetectors are a promising new step for next-generation light sensing across both visible and SWIR regimes at room temperature, with applications in imaging, surveillance, and communications.

### Supporting Information

Supporting Information is available from the Wiley Online Library or from the author.

### Acknowledgement

The authors acknowledge financial support from the Engineering and Physical Sciences Research Council (EPSRC) U.K. and the European Commission Horizon 2020 Framework (INFORM ITN).

### Conflict of Interest

The authors declare no conflict of interest.

## Keywords

dye, near-infrared, perovskite, photodiode, short-wavelength infrared

Received: May 9, 2017

Revised: July 11, 2017

Published online: August 4, 2017

- [1] G. Konstantatos, E. H. Sargent, *Nat. Nanotechnol.* **2010**, *5*, 391.
- [2] A. Rogalski, J. Antoszewski, L. Faraone, *J. Appl. Phys.* **2009**, *105*, 091101.
- [3] F. P. G. de Arquer, A. Armin, P. Meredith, E. H. Sargent, *Nat. Rev. Mater.* **2017**, *2*, 16100.
- [4] S. A. McDonald, G. Konstantatos, S. Zhang, P. W. Cyr, E. J. Klem, L. Levina, E. H. Sargent, *Nat. Mater.* **2005**, *4*, 138.
- [5] B. Jalali, S. Fathpour, *J. Lightwave Technol.* **2006**, *24*, 4600.
- [6] Z. Huang, J. E. Carey, M. Liu, X. Guo, E. Mazur, J. C. Campbell, *Appl. Phys. Lett.* **2006**, *89*, 033506.
- [7] M. Young, J. Suddard-Bangsund, T. J. Patrick, N. Pajares, C. J. Traverse, M. C. Barr, S. Y. Lunt, R. R. Lunt, *Adv. Opt. Mater.* **2016**, *4*, 1028.
- [8] A. Rogalski, *Infrared Phys. Technol.* **2002**, *43*, 187.
- [9] N. Huo, S. Gupta, G. Konstantatos, *Adv. Mater.* **2017**, *29*, 1606576.
- [10] W. Wang, F. Zhang, M. Du, L. Li, M. Zhang, K. Wang, Y. Wang, B. Hu, Y. Fang, J. Huang, *Nano Lett.* **2017**, *73*, 1995.
- [11] J. Miao, F. Zhang, Y. Lin, W. Wang, M. Gao, L. Li, J. Zhang, X. Zhan, *Adv. Opt. Mater.* **2016**, *4*, 1711.
- [12] W. Wang, F. Zhang, H. Bai, L. Li, M. Gao, M. Zhang, X. Zhan, *Nanoscale* **2016**, *8*, 5578.
- [13] G. Konstantatos, I. Howard, A. Fischer, S. Hoogland, J. Clifford, E. Klem, L. Levina, E. H. Sargent, *Nature* **2006**, *442*, 180.
- [14] J. P. Clifford, G. Konstantatos, K. W. Johnston, S. Hoogland, L. Levina, E. H. Sargent, *Nat. Nanotechnol.* **2009**, *4*, 40.
- [15] J. Feng, X. Yan, Y. Liu, H. Gao, Y. Wu, B. Su, L. Jiang, *Adv. Mater.* **2017**, *29*, 1605993.
- [16] L. Shen, Y. Fang, D. Wang, Y. Bai, Y. Deng, M. Wang, Y. Lu, J. Huang, *Adv. Mater.* **2016**, *28*, 10794.
- [17] M. I. Saidaminov, V. Adinolfi, R. Comin, A. L. Abdelhady, W. Peng, I. Dursun, M. Yuan, S. Hoogland, E. H. Sargent, O. M. Bakr, *Nat. Commun.* **2015**, *6*, 8724.
- [18] X. Hu, X. Zhang, L. Liang, J. Bao, S. Li, W. Yang, Y. Xie, *Adv. Funct. Mater.* **2014**, *24*, 7373.
- [19] W. Zhang, G. E. Eperon, H. J. Snaith, *Nat. Energy* **2016**, *1*, 16048.
- [20] S. D. Stranks, H. J. Snaith, *Nat. Nanotechnol.* **2015**, *10*, 391.
- [21] J. B. Patel, J. Wong-Leung, S. Van Reenen, N. Sakai, J. T. W. Wang, E. S. Parrott, M. Liu, H. J. Snaith, L. M. Herz, M. B. Johnston, *Adv. Electron. Mater.* **2016**, *3*, 1600470.
- [22] L. M. Herz, *ACS Energy Lett.* **2017**, *2*, 1539.
- [23] M. B. Johnston, L. M. Herz, *Acc. Chem. Res.* **2015**, *49*, 146.
- [24] L. M. Herz, *Ann. Rev. Phys. Chem.* **2016**, *67*, 65.
- [25] Q. Lin, A. Armin, D. M. Lyons, P. L. Burn, P. Meredith, *Adv. Mater.* **2015**, *27*, 2060.
- [26] Q. Lin, A. Armin, P. L. Burn, P. Meredith, *Nat. Photonics* **2015**, *9*, 687.
- [27] B. Murali, M. I. Saidaminov, A. L. Abdelhady, W. Peng, J. Liu, J. Pan, O. M. Bakr, O. F. Mohammed, *J. Mater. Chem. C* **2016**, *4*, 2545.
- [28] L. Dou, Y. M. Yang, J. You, Z. Hong, W.-H. Chang, G. Li, Y. Yang, *Nat. Commun.* **2014**, *5*, 5404.
- [29] M. I. Saidaminov, M. Haque, M. Savoie, A. L. Abdelhady, N. Cho, I. Dursun, U. Buttner, E. Alarousu, T. Wu, O. M. Bakr, *Adv. Mater.* **2016**, *28*, 8144.
- [30] Y. Fang, Q. Dong, Y. Shao, Y. Yuan, J. Huang, *Nat. Photonics* **2015**, *9*, 679.
- [31] S. Yakunin, M. Sytnyk, D. Kriegner, S. Shrestha, M. Richter, G. J. Matt, H. Azimi, C. J. Brabec, J. Stangl, M. V. Kovalenko, *Nat. Photonics* **2015**, *9*, 444.
- [32] Y. Liu, J. Sun, Z. Yang, D. Yang, X. Ren, H. Xu, Z. Yang, S. F. Liu, *Adv. Opt. Mater.* **2016**, *4*, 1829.
- [33] Q. Lin, A. Armin, P. L. Burn, P. Meredith, *Laser Photonics Rev.* **2016**, *10*, 1047.
- [34] W. Deng, L. Huang, X. Xu, X. Zhang, X. Jin, S.-T. Lee, J. Jie, *Nano Lett.* **2017**, *17*, 2482.
- [35] G. Lin, Y. Lin, H. Huang, R. Cui, X. Guo, B. Liu, J. Dong, X. Guo, B. Sun, *Nano Energy* **2016**, *27*, 638.
- [36] X. Zhang, S. Yang, H. Zhou, J. Liang, H. Liu, H. Xia, X. Zhu, Y. Jiang, Q. Zhang, W. Hu, *Adv. Mater.* **2017**, *29*, 1604431.
- [37] C.-j. Teng, D. Xie, M.-x. Sun, S. Chen, P. Yang, Y.-l. Sun, *ACS Appl. Mater. Interfaces* **2016**, *8*, 31289.
- [38] D. P. McMeekin, G. Sadoughi, W. Rehman, G. E. Eperon, M. Saliba, M. T. Hörlantner, A. Haghighirad, N. Sakai, L. Korte, B. Rech, *Science* **2016**, *351*, 151.
- [39] Z. Wang, D. P. McMeekin, N. Sakai, S. van Reenen, K. Wojciechowski, J. B. Patel, M. B. Johnston, H. J. Snaith, *Adv. Mater.* **2017**, *29*, 1604186.
- [40] Z. Li, M. Yang, J.-S. Park, S.-H. Wei, J. J. Berry, K. Zhu, *Chem. Mater.* **2015**, *28*, 284.
- [41] W. Rehman, D. P. McMeekin, J. B. Patel, R. L. Milot, M. B. Johnston, H. J. Snaith, L. M. Herz, *Energy Environ. Sci.* **2017**, *10*, 361.
- [42] W. Rehman, R. L. Milot, G. E. Eperon, C. Wehrenfennig, J. L. Boland, H. J. Snaith, M. B. Johnston, L. M. Herz, *Adv. Mater.* **2015**, *27*, 7938.
- [43] N. J. Jeon, J. H. Noh, W. S. Yang, Y. C. Kim, S. Ryu, J. Seo, S. I. Seok, *Nature* **2015**, *517*, 476.
- [44] J. Suddard-Bangsund, C. J. Traverse, M. Young, T. J. Patrick, Y. Zhao, R. R. Lunt, *Adv. Energy Mater.* **2016**, *6*, 1501659.
- [45] A. Armin, M. Hamsch, I. K. Kim, P. L. Burn, P. Meredith, E. B. Namdas, *Laser Photonics Rev.* **2014**, *8*, 924.
- [46] L. Shen, Y. Lin, C. Bao, Y. Bai, Y. Deng, M. Wang, T. Li, Y. Lu, A. Gruverman, W. Li, *Mater. Horiz.* **2017**, *4*, 242.